## RESEARCH ARTICLE

# Highly oxidized U(VI) within the smallest fullerene: gas-phase synthesis and computational study of boron-doped U@C$_{27}$B†

Antonio Moreno-Vicente,[a] Marc Alías-Rodríguez,[a,d] Paul W. Dunk,[b]
Coen de Graaf, [iD] *[a,c] Josep M. Poblet [iD] [a] and Antonio Rodríguez-Fortea [iD] *[a]

The smallest borafullerene U@C$_{27}$B has been synthesized using a laser vaporization cluster source and detected as the most abundant species in the U@C$_{2n-1}$B family. Density functional theory (DFT) calculations show that the U atom is placed just at the center of the cage interacting almost in the same way with all its atoms as if the cage were a 28-hapto ligand. Besides, the spin density is not at the metal, but distributed over the cage indicating that U is formally U(VI), even though it is not bonded to very electronegative atoms like O, F, N or Cl. All in all, we have synthesized a rather exotic radical that is another example of the distinctive host−guest chemistry that appears in endohedral metallofullerenes.

## 1. Introduction

Replacing a carbon atom in the fullerene cage by a heteroatom modifies the electronic structure of the fullerenes and hence their properties. The first heterofullerenes, detected only six years after the discovery of C$_{60}$,[1] were obtained as boron-doped carbon cages C$_{60-x}$B$_x$ by laser vaporization of graphite and boron nitride.[2] Indeed, boron and nitrogen are the preferred elements to dope fullerenes since they resemble carbon in size and electronegativity and are therefore most likely to form covalent bonds within the cage structure. Nitrogen-containing fullerenes have received more investigation than boron-doped cages because rational synthetic routes for the former were devised.[3–7] Production of macroscopic quantities of boron-doped C$_{60-x}$B$_x$ by arc burning was achieved in the late 90's.[8,9] In 2013, Kroto and co-workers reported the formation of borafullerenes by direct exposure of pristine C$_{60}$ (and C$_{70}$) to boron vapor by means of pulsed laser vaporization cluster source.[10] The C$_{59}$B radical, with the unpaired electron delocalized over the carbon cage, was predicted to have a high electron affinity so as to get reduced and become a closed-shell anion. A year

before, the same group had synthesized and detected the smallest fullerene known so far, the C$_{28}$ cage, which needs to be stabilized by the encapsulation of electropositive metals that donate four electrons to the cage, M@C$_{28}$ (with M = Ti, Zr, Hf and also U).[11] In fact, they also detected other "magic" peaks for the U@C$_{2n}$ series at C$_{36}$ and C$_{44}$ and concluded that the formation of endohedral mono-metallofullerenes M@C$_{2n}$ is directed by charge transfer, *i.e.* the smaller the carbon cage the larger the formal transfer to get the M@C$_{2n}$ stabilized.[12]

Other gas-phase detections of uranofullerenes[13,14] and computational studies on the U-cage interaction in small cages[15,16] or U–U bond in U$_2$@C$_{60}$ have been reported.[17] However, it was not until 2017 that the first actinidofullerene was synthesized by an arc-discharge method and fully characterized.[18] In Th@C$_{3v}$(8)-C$_{82}$, there is a formal transfer of four electrons from Th to the cage, in contrast to the three electrons transferred in lanthanide counterparts as La@C$_{2v}$(9)-C$_{82}$. The same year, three mono-uranofullerenes, U@D$_{3h}$-C$_{74}$, U@C$_2$(5)-C$_{82}$ and U@C$_{2v}$(9)-C$_{82}$ were also obtained and characterized, which provided the first observation of cage isomer dependent charge transfer states for U.[19] Since then, many other mono- and di-actinidofullerenes have been obtained, as for example U@C$_1$(17418)-C$_{76}$, U@C$_1$(28324)-C$_{80}$ and Th@C$_1$(28324)-C$_{80}$ in cages that do not obey the isolated pentagon rule (IPR),[20] U$_2$@I$_h$(7)-C$_{80}$,[21] or more recently U@C$_s$(6)-C$_{82}$, U@C$_2$(8)-C$_{84}$, U@C$_s$(15)-C$_{84}$, U@C$_1$(12)-C$_{86}$, Th@D$_{5h}$(6)-C$_{80}$ and Th$_2$@I$_h$(7)-C$_{80}$, among others.[22–24] The carbon cages can be used as effective nanocontainers to study the elusive actinide-actinide bond,[25,26] as for example in Th$_2$@I$_h$(7)-C$_{80}$,[24] or to encapsulate reactive or rare actinide clusters as in U$_2$N@I$_h$(7)-C$_{80}$,

*[a] Departament Química Física i Inorgànica, Universitat Rovira i Virgili, C/Marcel·lí Domingo 1, 43007 Tarragona, Spain. E-mail: antonio.rodriguezf@urv.cat*
*[b] National High Magnetic Field Laboratory, Florida State University, 1800 East Paul Dirac Drive, Tallahassee, FL 32310, USA*
*[c] ICREA, Pg Lluis Companys 23, 08010 Barcelona, Spain*
*[d] Aix-Marseille Univ, CNRS, ICR, Marseille, France*

$U_2C@I_h(7)$-$C_{80}$, $U_2C_2@I_h(7)$-$C_{80}$, $U_2C_2@D_{3h}(5)$-$C_{78}$ and $UCN@C_s(6)$-$C_{82}$.[27–30] The encapsulated actinides show a wide range of oxidation states, especially uranium, which is present as (i) U(v) in $U_2C@I_h(7)$-$C_{80}$; (ii) U(IV) in $U_2C_2@I_h(7)$-$C_{80}$ or $U@C_1(28324)$-$C_{80}$ and most of the mono-uranofullerenes; and (iii) U(III) in $U_2@I_h(7)$-$C_{80}$, $U@C_{2v}(9)$-$C_{82}$ or $UCN@C_s(6)$-$C_{82}$, for which the authors claimed an ambiguous oxidation state, U(III) *vs.* U(I).[28] The shortest U···C distances in all these uranofullerenes range between 2.40 and 2.55 Å, slightly shorter than in uranocene $U(\eta^8$-$C_8H_8)_2$, $U(\eta^5$-$C_5H_5)_4$ or in arene-bridged diuranium complexes.[31,32]

Herein, using a laser vaporization cluster source, we aim to prepare and characterize boron-doped $U@C_{2n-1}B$ endohedrals that can be scaled up for macroscopic production as well as have new properties and are attractive for applications. First, we describe the gas-phase synthesis and detection of boron-doped uranium endohedral fullerenes, along with the computational details of the calculations, and then we discuss the results. Two remarkable features are found in the smallest $U@C_{27}B$: (i) highly-oxidized U(VI) formal state; and (ii) large hapticity of the nanocontainer ligand.

## 2. Experimental

### 2.1. Gas-phase synthesis of $U@C_{2n-1}B$

The starting materials, graphite (99.9999%), boron powder (96%) and $UO_2$, are thoroughly mixed and then molded into a composite rod by compression. The optimal carbon target composition for boron-doped uranofullerene formation is found to be 0.8% U (atomic percent) and 10% B (atomic percent). $U@C_{2n-1}B$ are formed *in situ* by use of a pulsed supersonic cluster source by a single laser pulse of a Nd:YAG laser (532 nm, 5 mj per pulse) under a flow of helium.[12,33] The gas-phase reaction products were analysed by a custom-built 9.4 T FT-ICR mass spectrometer directly coupled to the cluster source and are conducted with positive ions.[34] Ions produced by 10 individual vaporization events were accumulated and transferred by octopoles to an open cylindrical trap ICR cell. The ions are then accelerated to a detectable radius by a broadband frequency sweep excitation, and detected as the differential current induced between two opposed electrodes of the ICR cell. The positively charged molecular ions are expected to be representative of the neutral abundance distribution generated by laser vaporization. Although, we note that the corresponding neutrals may exhibit different stabilities.

### 2.2. Computational details

The geometry optimizations were performed at density functional theory (DFT) level with the ADF 2018 program using different functionals (see ESI†).[35,36] The exchange–correlation hybrid functional PBE0 and the Slater TZP basis sets were used (PBE0/TZP) for the analysis.[37–39] Frozen cores consisting of (i) the 1s shell for C and B; (ii) the 1s to 5d shells for U were used. Relativistic corrections were included by means of the ZORA formalism. In addition, the Grimme Dispersion D3 method was considered.[40]

CASSCF/CASPT2 calculations were carried out using OpenMolcas 20.10.[41] The basis sets used were taken from the ano-rcc internal basis set library using the following contractions: (9s8p7d5f2g1h) for U and (4s3p1d) for C and B. No symmetry restrictions were imposed and Cholesky decomposition was employed to speed up the handling of two-electron integrals. Scalar relativistic effects were included through the Douglas–Kroll–Hess Hamiltonian. The molecular orbitals were optimized for the lowest 10 roots of each multiplicity in a state-average (SA-CASSCF) calculation. The active space contains 7 electrons distributed in all the possible ways over 13 molecular orbitals, including all the f-type U orbitals and six orbitals of the cage (Fig. S1†). Some of the active orbitals are clearly localized on U or the cage, but others are delocalized over the cage and U, which hampers the electron count on U, and makes it difficult to assign an oxidation state to the metal ion. To accurately determine the oxidation of each electronic state, we have localized the orbitals performing an orthonormal transformation of the MO in the active space.[42] The new set of orbitals (Fig. S2†) are localized on U or the cage with small orthogonalization tails onto the metal. Re-expressing the multiconfigurational wave function in this set of localized orbitals allows a direct determination of the number of electrons associated to U. The number of electrons in each localized orbital, the total number of electrons over U atom and the CASSCF energy can be found in Table S1.† Despite the accurate analysis that can be performed using a CASSCF wave function, the energies are commonly far from being correct because of the lack of dynamic electron correlation. These effects were added applying the second order perturbative correction to all electrons except the deep core ones to the CASSCF reference wave function, in the so-called single-state (SS-CASPT2) calculation. The standard 0.25 $E_h$ IPEA shift was used and the imaginary level shift was fixed at 0.05 $E_h$ to avoid the presence of weak *intruder states*. The influence of the imaginary level shift in the relative energies has also been tested (Fig. S3†).

## 3. Results and discussion

Fig. 1 shows that $U@C_{27}B$ forms as the smallest and most abundant species in the $U@C_{2n-1}B$ borafullerene family under our conditions, which is in agreement with the known smallest cage all-carbon analogue.[11] Other much less abundant peaks are also observed for $U@C_{35}B$, $U@C_{43}B$ and $U@C_{49}B$. To better understand this result, we have analysed the geometry and the electronic structure of $U@C_{27}B$. Due to the high symmetry of the cage ($T_d$), this fullerene shows only two positions for the substitution of a carbon atom by boron. It can be placed in the centre of three pentagon rings (also called 555 position) or in the centre of two pentagons and one hexagon (556). The energy difference found for these two isomers is 11.7 kcal $mol^{-1}$, with the 556 isomer lower in energy.
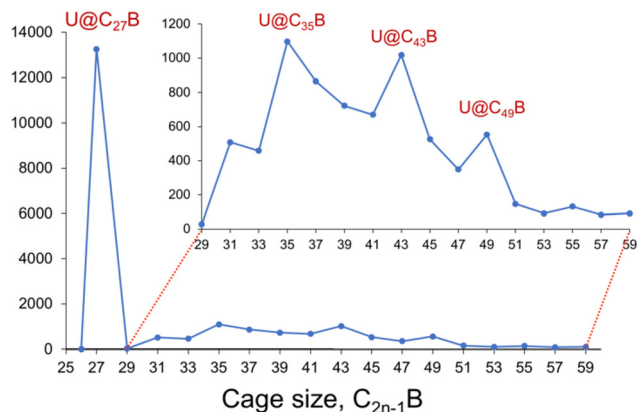
This journal is © the Partner Organisations 2023

*Inorg. Chem. Front.*, 2023, **10**, 908–914 | **909**

Fig. 1 Formation distribution (positive ions) for U@$C_{2n-1}$B products formed by laser vaporization of U-containing graphite starting material. Inset: the region $2n-1$ = 29 to 59 is expanded for clarity.



Fig. 3 Frontier molecular orbitals of U@$C_{27}$B at PBE0/TZP level. SOMO and LUMO are essentially cage orbitals and all U-5f orbitals are empty.

To confirm the endohedral position of U within the $C_{27}$B cage, we have computed some isomers with U coordinated to B and/or C atoms outside the cage (Table S5†). Those exohedral U-$C_{27}$B systems considered are more than 150 kcal mol$^{-1}$ higher in energy than U@$C_{27}$B. Interestingly, in U@$C_{27}$B the U atom is placed at the centre of the fullerene void interacting with all the 28 atoms of the cage in a very similar manner due to the small inner void and the large size of uranium, as compared for example with Ti@$C_{28}$, where Ti is off-centered.[11] All the C–U distances range between 2.41 and 2.53 Å, with the B–U distance being 2.51 Å (Fig. 2).

Neutral U@$C_{27}$B shows an unpaired electron, which is not located on the B atom, but mainly delocalized on the fullerene cage with a residual contribution on the internal U atom (see spin density in Fig. S4†). The oxidation potential is low in line with the high energy of the singly-occupied molecular orbital (SOMO, Fig. 3). Besides, it is remarkable that uranium atom formally transfers all its six valence electrons to the fullerene cage, as can be seen from an analysis of the electronic structure where all 5f orbitals of uranium are empty (Fig. 3). The doublet with the U(v) f$^1$ configuration is at 3.8 kcal mol$^{-1}$. It is

then one very rare example in which the formal oxidation state +6 of uranium is stabilized without the presence of highly electronegative atoms as oxygen, nitrogen, chlorine or fluorine.

We have confirmed this result by using multi-configurational wave-function based methods, CASSCF/CASPT2 (see Computational methods for details). The lowest-energy doublet, with formally 5f$^0$ U(vi), is 7.3 kcal mol$^{-1}$ lower in energy than the lowest doublet with 5f$^1$ U(v) electronic configuration (Table S1†). The charge distribution on the cage atoms, according to the Bader's Quantum Theory of Atoms in Molecules (QTAIM),[43] is found to be highly unequal, particularly around the heteroatom, as a consequence of their different electronegativities. The B atom bears a significant positive charge (+1.79) while the three C atoms directly bonded to it accumulate each an important negative charge (−0.65, −0.63 and −0.62) as compared to the low charge in the remaining 24 C atoms of the cage (around −0.05), see Fig. 4.
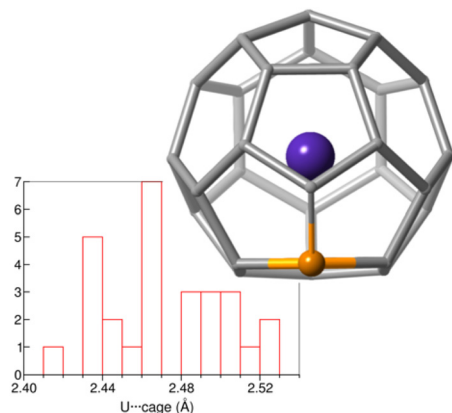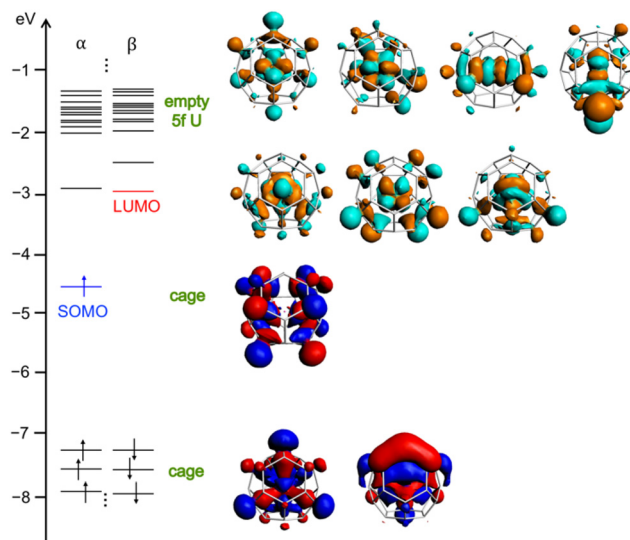


Fig. 2 Histogram of the U-cage distances in the optimized structure of U@$C_{27}$B. Besides, the optimized structure for the isomer 556 is shown.
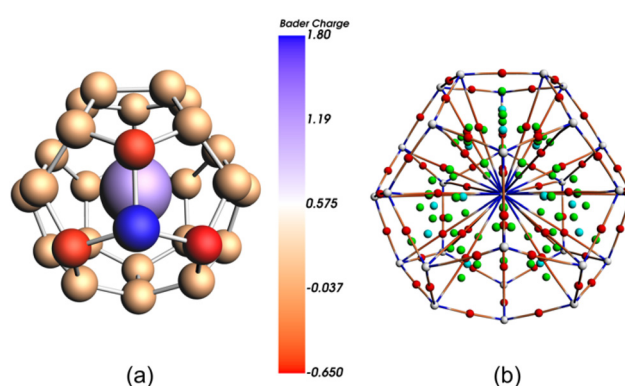


Fig. 4 Bader charges (a) and AIM critical points (CP) and bond paths (b) for U@$C_{27}$B. Atom CP in white, bond CP in red, ring CP in green and cage CP in light blue.

Localization index (LI), a QTAIM-based index that defines the population of an atomic basin minus the shared electrons, has been used recently to measure the oxidation state of electropositive atoms.[44,45] The difference between the LI and atomic number provides a measure of the charge of an atom after the ionic approximation for heteroatomic bonds, which corresponds to the IUPAC definition of oxidation state. Measure of $LI_U$ in $U@C_{27}B$ also confirms the U(VI) oxidation state. Furthermore, QTAIM was used to characterize the U-cage interactions. The *bond critical point* (bcp) postulated by Bader between two atoms is a necessary and sufficient condition for the atoms to be bonded. We have found 28 U-cage bcp, one for each of the 27 U–C interactions as well as for U–B (Fig. 4b). At these bcp, the corresponding values of electron density $\rho_{bcp}$ and Laplacian of the electron density $\nabla^2\rho_{bcp}$ are displayed in Table S3.†

As found for M-cage interactions in larger cages,[46] densities $\rho_{bcp}$ are around 0.5 $e\text{Å}^{-3}$ and values of the Laplacian $\nabla^2\rho_{bcp}$ are positive about 4–5 $e\text{Å}^{-5}$. Ring critical points (rcp) in the middle of the triangle formed by two contiguous U–C bcp and a C–C bcp are also found (Fig. S7†). Delocalization indices, $\delta$(U-cage), which provide a quantitative measure of the degree of electron sharing between the U atom and the cage and have been proposed as a measure of bond order,[47] are found to be around 0.3 for U–C interactions (Table S6†) and somewhat smaller, albeit non negligible, for the U–B interaction (0.097, Table S6†). From this topological analysis of the electron density and the histogram of the U–C distances, we can see the $C_{27}B$ cage that encapsulates U as if it were a ligand with a unusual very large hapticity ($\eta^{28}$).

Besides, we have analysed the electronic structure of $U@C_{27}B^+$ cation, since this is the species detected in the mass spectrometer when working in the positive mode. This cation, still with U(VI) oxidation state, is a rather stable closed-shell species with a considerably high HOMO–LUMO gap (4.92 eV at PBE0 level). CASPT2 calculations confirm that the lowest-energy singlet, by more than 80 kcal $mol^{-1}$, is essentially described (67%) by a configuration with formally U(VI) (see Table S2 and Fig. S5†).

Electronic structure and U–C bond lengths suggest a strong interaction between the actinide and the carbon cage, with the metal acting very likely as a template in the formation of the endohedral fullerene, as it is presumed for other endofullerenes or clusterfullerenes as $Sc_3N@C_{80}$.[33,34,48] Indeed, the importance of the metal–ligand interaction is clearly shown in the larger monometallic EMFs, where the U ion never remains in the centre of the cavity, but moves to the wall of the carbon cage.[19,20,23] This behaviour is general and does not depend on the metal type. The nature of the interaction is not very different from that observed in classical organometallic ligands.[31,32,49–51]

Finally, we have analysed the hypothetical system $Pa@C_{27}B$, isoelectronic to $U@C_{27}B^+$ with a closed-shell structure. Protactinium, with a very similar size as U, has the same spatial constraints and it is placed at the centre of the cage interacting with boron and all the carbon atoms in a quite similar way. The distance between the protactinium and the boron atom is 2.59 Å while the carbon–protactinium distances range between 2.45 and 2.58 Å (Fig. S6†). From an analysis of the electronic structure, we find that there is a huge gap between the HOMO and LUMO energy levels (3.93 eV, see Fig. S7†). As for $U@C_{27}B$, the metal transfers all its valence electrons, now five of them, to the fullerene cage, as shown by the seven empty 5f orbitals of protactinium with the HOMO belonging to the carbon cage. So, in this case the system can be seen, within the ionic model, as $Pa^{5+}@C_{27}B^{5-}$. Analysis of the critical points show that there is one bcp for each Pa–C interaction, but no bcp is found now for Pa–B (Table S4†). Delocalization indices, $\delta$(Pa–C), are around 0.25 and $\delta$(Pa–B) = 0.073.

## 4. Conclusions

The smallest fullerene observed so far, $M@C_{28}$ (M = Ti, Zr and U), is boron-doped in the form $U@C_{27}B$ using laser vaporization techniques and detected by high resolution FT-ICR mass spectrometry as the most abundant borafullerene in the $U@C_{2n-1}B$ family. The large size of the actinide combined with the small inner void inside $C_{27}B$ enforces the U atom to be placed in the middle of the cage in such a way that the interaction with all 28 atoms is optimized and the encapsulation can be seen as a 28-hapto interaction with the cage. Significant asymmetry in charges is observed around the heteroatom, which is positively charged, with the three C atoms directly bonded to it that keep most of the negative charge. From a detailed analysis of the electronic structure uranium can be formally described as highly oxidized U(VI), $U^{6+}@C_{27}B^{6-}$, even though no bond to very electronegative atoms like O, F, N or Cl exists. This inorganic radical that is formed in the gas phase, remains very abundant when detected as $U@C_{27}B^+$ in the positive mode of the mass spectrometer, once one electron is lost and a large-gap closed shell structure is obtained. Stabilization by forming charge-transfer complexes with electron acceptors would be expected for this $U@C_{27}B$ bizarre radical, which is another example of the special host–guest interaction in endohedral metallofullerenes.

## Author contributions

A.M.-V. investigation, formal analysis, methodology, visualization, writing – original draft; M.A.-R. investigation, formal analysis, methodology; P.W.D. conceptualization, investigation, methodology, validation, writing – review & editing; C.d.G. conceptualization, funding acquisition, supervision, writing – review & editing; J.M.P. conceptualization, funding acquisition, supervision, writing – review & editing; A.R.-F. conceptualization, investigation, formal analysis, funding acquisition, supervision, writing – original draft; writing – review & editing.

This journal is © the Partner Organisations 2023

*Inorg. Chem. Front.*, 2023, **10**, 908–914 | **911**

## Conflicts of interest

There are no conflicts to declare.

## Acknowledgements

## References

1  H. W. Kroto, J. R. Heath, S. C. O'Brien, R. F. Curl and R. E. Smalley, $C_{60}$ - Buckminsterfullerene, *Nature*, 1985, **318**, 162–163.

2  T. Guo, C. M. Jin and R. E. Smalley, Doping Bucky - Formation and Properties of Boron—Doped Buckminsterfullerene, *J. Phys. Chem.*, 1991, **95**, 4948–4950.

3  J. C. Hummelen, B. Knight, J. Pavlovich, R. Gonzalez and F. Wudl, Isolation of the Heterofullerene $C_{59}N$ As Its Dimer $(C_{59}N)_2$, *Science*, 1995, **269**, 1554–1556.

4  M. Keshavarz-K, R. Gonzalez, R. G. Hicks, G. Srdanov, V. I. Srdanov, T. G. Collins, J. C. Hummelen, C. Bellavia-Lund, J. Pavlovich, F. Wudl and K. Holczer, Synthesis of Hydrozafullerene $C_{59}HN$, the Parent Hydroheterofullerene, *Nature*, 1996, **383**, 147–150.

5  I. Lamparth, B. Nuber, G. Schick, A. Skiebe, T. Grosser and A. Hirsch, $C_{59}N^+$ and $C_{69}N^+$ - Isoelectronic Heteroanalogues of $C_{60}$ and $C_{70}$, *Angew. Chem., Int. Ed. Engl.*, 1995, **34**, 2257–2259.

6  B. Nuber and A. Hirsch, A New Route to Nitrogen Heterofullerenes and the First Synthesis of $(C_{69}N)_2$, *Chem. Commun.*, 1996, 1421–1422.

7  N. N. Xin, H. Huang, J. X. Zhang, Z. F. Dai and L. B. Gan, Fullerene Doping: Preparation of Azafullerene $C_{59}NH$ and Oxafulleroids $C_{59}O_3$ and $C_{60}O_4$, *Angew. Chem., Int. Ed.*, 2012, **51**, 6163–6166.

8  B. P. Cao, X. H. Zhou, Z. J. Shi, Z. X. Jin, Z. N. Gu, H. Z. Xiao and J. Z. Wang, Synthesis and Characterization of Boron-Doped Fullerenes, *Acta Phys.–Chim. Sin.*, 1997, **13**, 204–206.

9  H. J. Muhr, R. Nesper, B. Schnyder and R. Kotz, The Boron Heterofullerenes $C_{59}B$ and $C_{69}B$: Generation, Extraction, Mass Spectrometric and XPS Characterization, *Chem. Phys. Lett.*, 1996, **249**, 399–405.

10  P. W. Dunk, A. Rodriguez-Fortea, N. K. Kaiser, H. Shinohara, J. M. Poblet and H. W. Kroto, Formation of Heterofullerenes by Direct Exposure of $C_{60}$ to Boron Vapor, *Angew. Chem., Int. Ed.*, 2013, **52**, 315–319.

11  P. W. Dunk, N. K. Kaiser, M. Mulet-Gas, A. Rodriguez-Fortea, J. M. Poblet, H. Shinohara, C. L. Hendrickson, A. G. Marshall and H. W. Kroto, The Smallest Stable Fullerene, $M@C_{28}$ (M=Ti, Zr, U): Stabilization and Growth from Carbon Vapor, *J. Am. Chem. Soc.*, 2012, **134**, 9380–9389.

12  P. W. Dunk, M. Mulet-Gas, Y. Nakanishi, N. K. Kaiser, A. Rodriguez-Fortea, H. Shinohara, J. M. Poblet, A. G. Marshall and H. W. Kroto, Bottom-up Formation of Endohedral Mono-Metallofullerenes is Directed by Charge Transfer, *Nat. Commun.*, 2014, **5**, 5844.

13  M. D. Diener, C. A. Smith and D. K. Veirs, Anaerobic Preparation and Solvent-Free Separation of Uranium Endohedral Metallofullerenes, *Chem. Mater.*, 1997, **9**, 1773–1777.

14  A. Gomez-Torres, R. Esper, P. W. Dunk, R. Morales-Martinez, A. Rodriguez-Fortea, L. Echegoyen and J. M. Poblet, Small Cage Uranofullerenes: 27 Years after Their First Observation, *Helv. Chim. Acta*, 2019, **102**, e1900046.

15  X. Dai, Y. Gao, W. Jiang, Y. Lei and Z. Wang, $U@C_{28}$: The Electronic Structure Induced by the 32-Electron Principle, *Phys. Chem. Chem. Phys.*, 2015, **17**, 23308–23311.

16  J.-P. Dognon, C. Clavaguera and P. Pyykko, A Predicted Organometallic Series Following a 32-Electron Principle: $An@C_{28}$ (An=Th, $Pa^+$, $U^{2+}$, $Pu^{4+}$), *J. Am. Chem. Soc.*, 2009, **131**, 238–243.

17  X. Wu and X. Lu, Dimetalloendofullerene $U_2@C_{60}$ Has a U-U Multiple Bond Consisting of Sixfold One-Electron-Two-Center Bonds, *J. Am. Chem. Soc.*, 2007, **129**, 2171–2177.

18  Y. Wang, R. Morales-Martinez, X. Zhan, W. Yang, Y. Wang, A. Rodriguez-Fortea, J. M. Poblet, L. Feng, S. Wang and N. Chen, Unique Four-Electron Metal-to-Cage Charge Transfer of Th to a $C_{82}$ Fullerene Cage: Complete Structural Characterization of $Th@C_{3v}(8)$-$C_{82}$, *J. Am. Chem. Soc.*, 2017, **139**, 5110–5116.

19  W. Cai, R. Morales-Martinez, X. Zhang, D. Najera, E. L. Romero, A. Metta-Magana, A. Rodriguez-Fortea, S. Fortier, N. Chen, J. M. Poblet and L. Echegoyen, Single Crystal Structures and Theoretical Calculations of Uranium Endohedral Metallofullerenes $(U@C_{2n}, 2n=74, 82)$ Show Cage Isomer Dependent Oxidation States for U, *Chem. Sci.*, 2017, **8**, 5282–5290.

20  W. Cai, L. Abella, J. Zhuang, X. Zhang, L. Feng, Y. Wang, R. Morales-Martinez, R. Esper, M. Boero, A. Metta-Magana, A. Rodriguez-Fortea, J. M. Poblet, L. Echegoyen and N. Chen, Synthesis and Characterization of Non-Isolated-Pentagon-Rule Actinide Endohedral Metallofullerenes $U@C_1(17418)$-$C_{76}$, $U@C_1(28324)$-$C_{80}$, and $Th@C_1(28324)$-$C_{80}$: Low-Symmetry Cage Selection Directed by a Tetravalent Ion, *J. Am. Chem. Soc.*, 2018, **140**, 18039–18050.

21  X. Zhang, Y. Wang, R. Morales-Martinez, J. Zhong, C. de Graaf, A. Rodriguez-Fortea, J. M. Poblet, L. Echegoyen, L. Feng and N. Chen, $U_2@I_h(7)$-$C_{80}$: Crystallographic Characterization of a Long-Sought Dimetallic Actinide Endohedral Fullerene, *J. Am. Chem. Soc.*, 2018, **140**, 3907–3915.

22  Y. Yan, R. Morales-Martinez, J. Zhuang, Y.-R. Yao, X. Li, J. M. Poblet, A. Rodriguez-Fortea and N. Chen, $Th@D_{5h}(6)$-$C_{80}$: A Highly Symmetric Fullerene Cage Stabilized by a Single Metal Ion, *Chem. Commun.*, 2021, **57**, 6624–6627.

23 Y.-R. Yao, Y. Rosello, L. Ma, A. R. P. Santiago, A. Metta-Magana, N. Chen, A. Rodriguez-Fortea, J. M. Poblet and L. Echegoyen, Crystallographic Characterization of U@C$_{2n}$ (2n=82-86): Insights about Metal-Cage Interactions for Mono-metallofullerenes, *J. Am. Chem. Soc.*, 2021, **143**, 15309–15318.

24 J. Zhuang, R. Morales-Martinez, J. Zhang, Y. Wang, Y.-R. Yao, C. Pei, A. Rodriguez-Fortea, S. Wang, L. Echegoyen, C. de Graaf, J. M. Poblet and N. Chen, Characterization of a Strong Covalent Th$^{3+}$-Th$^{3+}$ Bond Inside an I$_h$(7)-C$_{80}$ Fullerene Cage, *Nat. Commun.*, 2021, **12**, 2372.

25 C. Foroutan-Nejad, J. Vicha, R. Marek, M. Patzschke and M. Straka, Unwilling U-U Bonding in U$_2$@C$_{80}$: Cage-Driven Metal-Metal Bonds in Di-Uranium Fullerenes, *Phys. Chem. Chem. Phys.*, 2015, **17**, 24182–24192.

26 A. Jaros, C. Foroutan-Nejad and M. Straka, From pi Bonds without sigma Bonds to the Longest Metal-Metal Bond Ever: A Survey on Actinide-Actinide Bonding in Fullerenes, *Inorg. Chem.*, 2020, **59**, 12608–12615.

27 X. Li, Y. Rosello, Y.-R. Yao, J. Zhuang, X. Zhang, A. Rodriguez-Fortea, C. de Graaf, L. Echegoyen, J. M. Poblet and N. Chen, U$_2$N@I$_h$(7)-C$_{80}$: Fullerene Cage Encapsulating an Unsymmetrical U(IV)=N=U(V) Cluster, *Chem. Sci.*, 2021, **12**, 282–292.

28 Q. Meng, L. Abella, W. Yang, Y.-R. Yao, X. Liu, J. Zhuang, X. Li, L. Echegoyen, J. Autschbach and N. Chen, UCN@C$_s$(6)-C$_{82}$: An Encapsulated Triangular UCN Cluster with Ambiguous U Oxidation State U(III) versus U(I), *J. Am. Chem. Soc.*, 2021, **143**, 16226–16234.

29 X. Zhang, W. Li, L. Feng, X. Chen, A. Hansen, S. Grimme, S. Fortier, D.-C. Sergentu, T. J. Duignan, J. Autschbach, S. Wang, Y. Wang, G. Velkos, A. A. Popov, N. Aghdassi, S. Duhm, X. Li, J. Li, L. Echegoyen, W. H. E. Schwarz and N. Chen, A Diuranium Carbide Cluster Stabilized Inside a C$_{80}$ Fullerene Cage, *Nat. Commun.*, 2018, **9**, 2753.

30 J. Zhuang, L. Abella, D.-C. Sergentu, Y.-R. Yao, M. Jin, W. Yang, X. Zhang, X. Li, D. Zhang, Y. Zhao, X. Li, S. Wang, L. Echegoyen, J. Autschbach and N. Chen, Diuranium(IV) Carbide Cluster U$_2$C$_2$ Stabilized Inside Fullerene Cages, *J. Am. Chem. Soc.*, 2019, **141**, 20249–20260.

31 P. L. Diaconescu, P. L. Arnold, T. A. Baker, D. J. Mindiola and C. C. Cummins, Arene-Bridged Diuranium Complexes: Inverted Sandwiches Supported by Delta Backbonding, *J. Am. Chem. Soc.*, 2000, **122**, 6108–6109.

32 B. Vlaisayljevich, P. L. Diaconescu, W. L. Lukens Jr., L. Gagliardi and C. C. Cummins, Investigations of the Electronic Structure of Arene-Bridged Diuranium Complexes, *Organometallics*, 2013, **32**, 1341–1352.

33 M. Mulet-Gas, L. Abella, M. R. Ceron, E. Castro, A. G. Marshall, A. Rodriguez-Fortea, L. Echegoyen, J. M. Poblet and P. W. Dunk, Transformation of Doped Graphite into Cluster-Encapsulated Fullerene Cages, *Nat. Commun.*, 2017, **8**, 1222.

34 P. W. Dunk, N. K. Kaiser, C. L. Hendrickson, J. P. Quinn, C. P. Ewels, Y. Nakanishi, Y. Sasaki, H. Shinohara, A. G. Marshall and H. W. Kroto, Closed Network Growth of Fullerenes, *Nat. Commun.*, 2012, **3**, 855.

35 ADF 2018, SCM, Theoretical Chemistry, Vrije Universiteit, Amsterdam, The Netherlands, **https://www.scm.com**.

36 G. T. te Velde, F. M. Bickelhaupt, E. J. Baerends, C. F. Guerra, S. J. A. Van Gisbergen, J. G. Snijders and T. Ziegler, Chemistry with ADF, *J. Comput. Chem.*, 2001, **22**, 931–967.

37 C. Adamo and V. Barone, Toward Reliable Density Functional Methods without Adjustable Parameters: The PBE0 Model, *J. Chem. Phys.*, 1999, **110**, 6158–6170.

38 M. Ernzerhof and G. E. Scuseria, Assessment of the Perdew-Burke-Ernzerhof Exchange-Correlation Functional, *J. Chem. Phys.*, 1999, **110**, 5029–5036.

39 E. Van Lenthe and E. J. Baerends, Optimized Slater-Type Basis Sets for the Elements 1-118, *J. Comput. Chem.*, 2003, **24**, 1142–1156.

40 S. Grimme, S. Ehrlich and L. Goerigk, Effect of the Damping Function in Dispersion Corrected Density Functional Theory, *J. Comput. Chem.*, 2011, **32**, 1456–1465.

41 I. Fdez. Galván, M. Vacher, A. Alavi, C. Angeli, F. Aquilante, J. Autschbach, J. J. Bao, S. I. Bokarev, N. A. Bogdanov, R. K. Carlson, L. F. Chibotaru, J. Creutzberg, N. Dattani, M. G. Delcey, S. S. Dong, A. Dreuw, L. Freitag, L. M. Frutos, L. Gagliardi, F. Gendron, A. Giussani, L. González, G. Grell, M. Guo, C. E. Hoyer, M. Johansson, S. Keller, S. Knecht, G. Kovačević, E. Källman, G. Li Manni, M. Lundberg, Y. Ma, S. Mai, J. P. Malhado, P. Å. Malmqvist, P. Marquetand, S. A. Mewes, J. Norell, M. Olivucci, M. Oppel, Q. M. Phung, K. Pierloot, F. Plasser, M. Reiher, A. M. Sand, I. Schapiro, P. Sharma, C. J. Stein, L. K. Sørensen, D. G. Truhlar, M. Ugandi, L. Ungur, A. Valentini, S. Vancoillie, V. Veryazov, O. Weser, T. A. Wesołowski, P.-O. Widmark, S. Wouters, A. Zech, J. P. Zobel and R. Lindh, OpenMolcas: From Source Code to Insight, *J. Chem. Theory Comput.*, 2019, **15**, 5925–5964.

42 A. Sadoc, R. Broer and C. de Graaf, Role of Charge Transfer Configurations in LaMnO$_3$, CaMnO$_3$, and CaFeO$_3$, *J. Chem. Phys.*, 2007, **126**, 134709.

43 R. F. W. Bader, *Atoms in Molecules: a Quantum Theory*, Clarendon Press, Oxford, 1990.

44 C. S. Day, C. D. Do, C. Odena, J. Benet-Buchholz, L. Xu, C. Foroutan-Nejad, K. H. Hopmann and R. Martin, Room-Temperature-Stable Magnesium Electride via Ni(II) Reduction, *J. Am. Chem. Soc.*, 2022, **144**, 13109–13117.

45 J. Mehara, A. K. Surendran, T. van Wieringen, D. Setia, C. Foroutan-Nejad, M. Straka, L. Rulisek and J. Roithova, Cationic Gold(II) Complexes: Experimental and Theoretical Study, *Chem. – Eur. J.*, 2022, **28**, e202201794.

46 A. A. Popov and L. Dunsch, Bonding in Endohedral Metallofullerenes as Studied by Quantum Theory of Atoms in Molecules, *Chem. – Eur. J.*, 2009, **15**, 9707–9729.

47 C. Outeiral, M. A. Vincent, A. Martín Pendás and P. L. A. Popelier, Revitalizing the Concept of Bond Order through Delocalization Measures in Real Space, *Chem. Sci.*, 2018, **9**, 5517–5529.

This journal is © the Partner Organisations 2023

*Inorg. Chem. Front.*, 2023, **10**, 908–914 | **913**

48 S. Stevenson, G. Rice, T. Glass, K. Harich, F. Cromer, M. R. Jordan, J. Craft, E. Hadju, R. Bible, M. M. Olmstead, K. Maitra, A. J. Fisher, A. L. Balch and H. C. Dorn, Small-Bandgap Endohedral Metallofullerenes in High Yield and Purity, *Nature*, 1999, **401**, 55–57.

49 W. Fang, Q. Zhu and C. Zhu, Recent Advances in Heterometallic Clusters with f-Block Metal–Metal Bonds: Synthesis, Reactivity and Applications, *Chem. Soc. Rev.*, 2022, **51**, 8434–8449.

50 J. K. Pagano, J. Xie, K. A. Erickson, S. K. Cope, B. L. Scott, R. Wu, R. Waterman, D. E. Morris, P. Yang, L. Gagliardi and J. L. Kiplinger, Actinide 2-Metallabiphenylenes That Satisfy Hückel's Rule, *Nature*, 2020, **578**, 563–567.

51 I. A. Popov, B. S. Billow, S. H. Carpenter, E. R. Batista, J. M. Boncella, A. M. Tondreau and P. Yang, An Allyl Uranium(IV) Sandwich Complex: Are φ Bonding Interactions Possible?, *Chem. – Eur. J.*, 2022, **28**, e202200114.